Cell

Foxa2 and H2A.Z Mediate Nucleosome Depletion during Embryonic Stem Cell Differentiation

Zhaoyu Li,[1] Paul Gadue,[2] Kaifu Chen,[3] Yang Jiao,[1] Geetu Tuteja,[1] Jonathan Schug,[1] Wei Li,[3] and Klaus H. Kaestner[1,*]
[1]Department of Genetics and Institute of Diabetes, Obesity and Metabolism, School of Medicine, University of Pennsylvania, Philadelphia, PA 19104, USA
[2]The Children's Hospital of Philadelphia, Philadelphia, PA 19104, USA
[3]Division of Biostatistics, Dan L. Duncan Cancer Center, Department of Molecular and Cellular Biology, Baylor College of Medicine, One Baylor Plaza, Houston, TX 77030, USA
*Correspondence: kaestner@mail.med.upenn.edu
http://dx.doi.org/10.1016/j.cell.2012.11.018

SUMMARY

Nucleosome occupancy is fundamental for establishing chromatin architecture. However, little is known about the relationship between nucleosome dynamics and initial cell lineage specification. Here, we determine the mechanisms that control global nucleosome dynamics during embryonic stem (ES) cell differentiation into endoderm. Both nucleosome depletion and de novo occupation occur during the differentiation process, with higher overall nucleosome density after differentiation. The variant histone H2A.Z and the winged helix transcription factor Foxa2 both act to regulate nucleosome depletion and gene activation, thus promoting ES cell differentiation, whereas DNA methylation promotes nucleosome occupation and suppresses gene expression. Nucleosome depletion during ES cell differentiation is dependent on Nap1l1-coupled SWI/SNF and INO80 chromatin remodeling complexes. Thus, both epigenetic and genetic regulators cooperate to control nucleosome dynamics during ES cell fate decisions.

INTRODUCTION

Next-generation sequencing technology has enabled the construction of genome-wide high-resolution maps for nucleosomes in human, rodent, nematode, and yeast genomes (Li et al., 2011; Schones et al., 2008; Shivaswamy et al., 2008; Valouev et al., 2008). Despite these advances, to date, the molecular mechanisms that drive nucleosome dynamics have not been fully elucidated. In addition, it is still debatable whether nucleosome occupancy changes during differentiation (Ho and Crabtree, 2010; Jiang and Pugh, 2009; Schones et al., 2008). Chromatin remodeling complexes and chaperones maintain the balance between nucleosome disassembly and assembly during transcriptional elongation (Clapier and Cairns, 2009), but it remains to be determined whether existing nucleosomes disappear or new nucleosomes assemble during cellular differentiation.

Directed differentiation of pluripotent embryonic stem (ES) cells into tissue-specific progenitor cells provides a valuable tool to dissect cell lineage decisions and to answer the questions raised above. By comparing undifferentiated with differentiated ES cells, genome-wide alterations in DNA methylation and histone modifications have been shown to accompany the differentiation process (Meissner et al., 2008; Mikkelsen et al., 2007). However, the impact of the fundamental architecture of chromatin, that is the nucleosome, on differentiation has not been determined at the genome-wide level.

The vertebrate forkhead box A (*Foxa*) factors, Foxa1, Foxa2, and Foxa3, have been suggested to act as ''pioneer'' factors in liver development based on in vitro studies demonstrating that Foxa proteins decompact chromatin and reposition nucleosomes at an *Albumin* enhancer construct in vitro (McPherson et al., 1993; Zaret, 1999). Interestingly, genetic studies have shown that no liver forms in mice when both *Foxa1* and *Foxa2* are ablated in the foregut endoderm following gastrulation (Lee et al., 2005). However, deletion of the two genes after liver specification does not affect chromatin structure and organ expansion (Li et al., 2011). These data suggest that Foxa1/2 act in chromatin remodeling only during early development. In addition, the variant histone H2A.Z has been suggested to be involved in histone exchange, and possibly in nucleosome eviction, and to be critical for ES cell differentiation (Lee et al., 2006; Mavrich et al., 2008; Mizuguchi et al., 2004).

Thus, we hypothesize that both Foxa2 and H2A.Z regulate nucleosome dynamics during ES cell differentiation. To test this hypothesis, we applied genome-wide high-resolution nucleosome mapping and chromatin immunoprecipitation sequencing (ChIP-Seq) to identify nucleosome dynamic regions and their correlation with Foxa2, H2A.Z, and chromatin remodeler occupancy during ES cell differentiation. Furthermore, we used gene suppression by RNAi to address the requirement of specific factors in the process of nucleosome dynamics and ES cell differentiation.

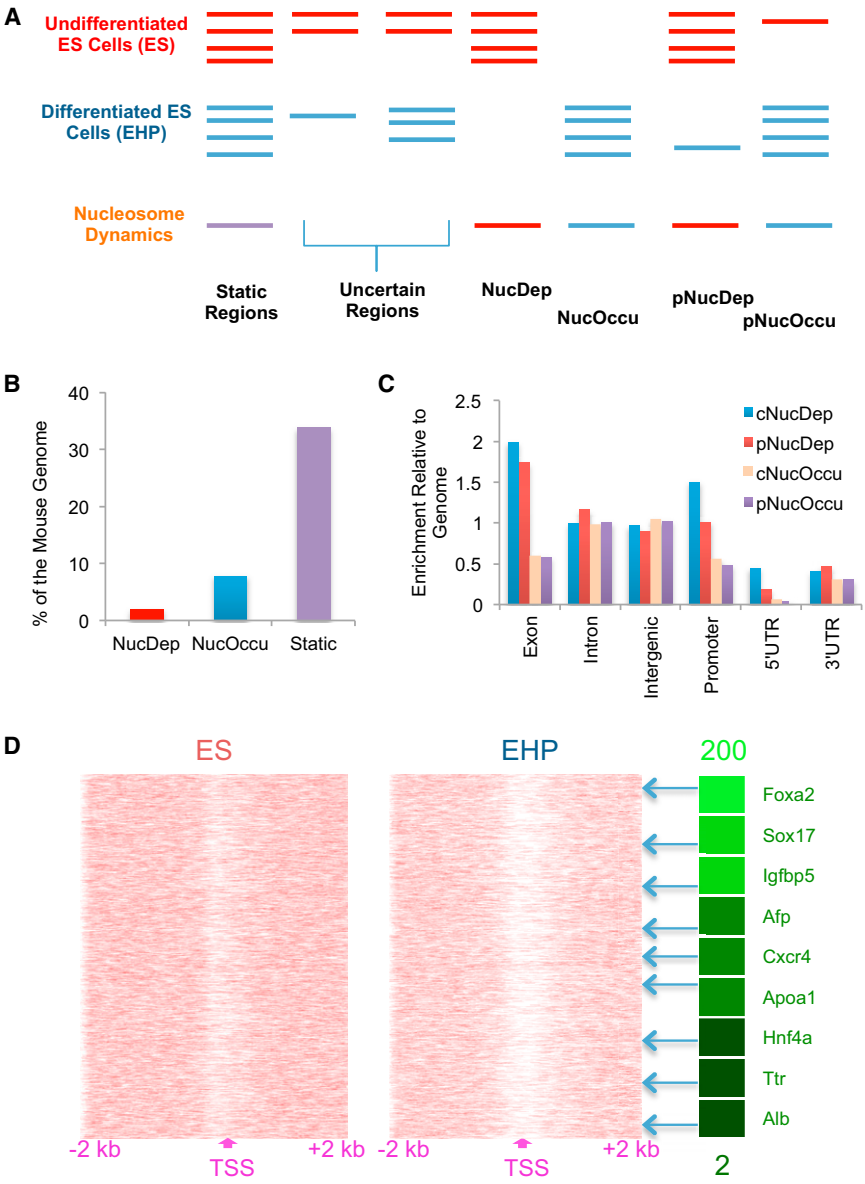

Figure 1. Nucleosome Dynamics during ES Cell Differentiation

(A) Schematic view of our computational analysis of nucleosome occupancy changes between undifferentiated ES and lineage-committed EHP cells. Red and blue lines represent nucleosome occupancy in undifferentiated and differentiated ES cells, respectively. The nucleosome-bound and dynamic regions were identified computationally by the algorithm DANPOS (Figure S1B). Complete and partial nucleosome depletion regions (NucDep and pNucDep) and complete and partial nucleosome occupation regions (NucOccu and pNucOccu) were further defined following the DANPOS analysis. "Complete" means no sequencing tags found in either ES or EHP cells; "partial" means sequencing tags found in both cell types, but with at least a 4-fold difference.

(B) Percentage of dynamic nucleosome regions in the whole genome during ES cell differentiation.

(C) Distribution of nucleosome dynamic regions in the genome is normalized to the genomic distribution of all regions. 1 equals the genomic distribution of each region. Genome, the whole mouse genome (mm8).

(D) Nucleosome distribution near TSS of the 2,000 most activated (by mRNA level) genes during ES cell differentiation. Genes with increased expression after differentiation exhibit nucleosome depletion near their TSS. The gene list includes key hepatic differentiation markers, and the green shading indicates the degree of gene activation as measured by fold change of mRNA levels (up to 200) between EHP and ES cells.

See also Figures S1 and S2.

RESULTS

Nucleosome Occupancy Is Dynamic during ES Cell Differentiation

We investigated nucleosome dynamics during differentiation of ES cells into the endoderm/hepatic fate, which can be directed in vitro using a cocktail of growth factors including BMP-4 and Activin A (Gadue et al., 2006; Gouon-Evans et al., 2006; Nostro et al., 2008) and tracked using a *Foxa2* promoter-driven CD4 replacement allele (Gadue et al., 2006). By combining selection for the Foxa2/CD4 marker and an endoderm-specific antibody (ENDM1) (Gadue et al., 2009), we sorted lineage-committed endoderm/hepatic progenitor (EHP) cells. Next, we mapped nucleosome positions genome-wide in ES and EHP cells by micrococcal nuclease (MNase) digestion followed by next-generation sequencing (MNase-Seq; see experimental setup outlined in Figure S1A available online). In total, ~150 million uniquely aligned sequence reads were obtained for each cell type (Table S1). We identified dynamic features in the genome where nucleosome occupancy differed between ES and EHP cells using the DANPOS algorithm (see Experimental Procedures and Figure S1B). We found "complete nucleosome depletion regions" (NucDep, changing from nucleosome occupied to nucleosome free during the course of differentiation), "complete nucleosome occupation regions" (NucOccu, changing from nucleosome free to nucleosome occupied), and partial nucleosome dynamic regions (Figure 1A). The remainder of the genome was defined as "static" (always bound by nucleosomes), "nucleosome free" (never occupied by nucleosomes), and "uncertain" (weakly bound by nucleosomes). Both nucleosome depletion and occupation occurred during the differentiation from ES to EHP cells, but nucleosome occupation was the more frequent event (Figure 1B), indicating that more nucleosomes bind the genome after ES cell differentiation. Regions of dynamic nucleosome were enriched at exon and promoter regions as compared to the whole mouse genome (Figure 1C).

To investigate the impact of nucleosome dynamics on gene regulation, we determined gene expression profiles for both ES and EHP cells. For genes that were activated during ES cell differentiation, we observed nucleosome depletion mainly between the transcriptional start site (TSS) and 1 kb downstream (Figure S2A). Consistent with previous studies (Jiang and Pugh, 2009; Schones et al., 2008), nucleosome deficiency at TSSs of highly expressed genes in each cell type correlated with gene activation in general (Figure S2A). To investigate the impact of nucleosome dynamics on ES cell differentiation, we plotted nucleosome occupancy near TSSs (Figure 1D): Clear nucleosome depletion was observed near TSSs for genes activated during the differentiation process, including endoderm and hepatic differentiation markers such as Foxa2, alpha-fetoprotein, and albumin. Thus, nucleosome depletion at TSSs correlates with activation of endoderm/hepatic genes during ES cell differentiation.

Foxa2 and H2A.Z Mediate Nucleosome Depletion during ES Cell Differentiation

To investigate the mechanisms involved in nucleosome depletion during ES cell differentiation, we analyzed the distribution of nucleosome depletion regions surrounding relevant histone variants and Foxa2 binding sites. Using ChIP-seq, we determined genome-wide locations of H2A.Z and H2A.X in undifferentiated ES cells, and of Foxa2 in fully differentiated EHP cells. H2A.Z was previously reported to mark the 5′ end of transcribed regions (Raisner et al., 2005). We found that H2A.Z flanked TSSs in a bimodal distribution, in contrast to H2A.X, which is depleted near TSSs (Figure S2B). Genome-wide location analysis also showed that H2A.Z and Foxa2, but not H2A.X, were enriched at exons and promoter regions (Figure S2C). By comparing nucleosome maps in ES and EHP cells, we found strong nucleosome depletion near Foxa2 binding sites during ES cell differentiation (Figure 2A). Nucleosome depletion, but not occupation, regions were enriched near H2A.Z binding sites in ES cells and Foxa2 binding sites in EHP cells, but not at H2A.X-enriched regions (Figures 2B and 2C), which suggests that nucleosomes containing H2A.Z in ES cells were preferentially lost during differentiation as compared to non-H2A.Z nucleosomes.

To investigate this dynamic process, we collected partially differentiated EHP (pEHP) cells (Figure S3A). We analyzed Foxa2 and H2A.Z occupancy in ES, pEHP, and EHP cells by ChIP-seq. The comparison of H2A.Z binding sites (pooled from ES and pEHP cells) with Foxa2 binding sites (pooled from pEHP and EHP cells) revealed that 2,412 Foxa2 binding sites colocalized with H2A.Z sites. Remarkably, of these 2,412 sites, 84% occurred at nucleosome depletion regions (Figure 2D). Further analysis showed that Foxa2 binding was strong at regions depleted of nucleosomes in EHP cells and to a lesser extent in pEHP cells (Figure 2E). It is important to note that H2A.Z binding near nucleosome depletion regions was reduced in pEHP cells and diminished in fully differentiated (EHP) cells (Figures 2F and 2G).

Genome-wide location analysis demonstrated a close correlation between Foxa2 in EHP and H2A.Z binding in ES cells (Figure 2G; Figure S2D). These findings suggested that co-occupancy of Foxa2 and H2A.Z at relevant nucleosomes occurrs in the transition between undifferentiated and differentiated ES cells. In fact, using pEHP cells, we could capture this transition state by sequential chip for Foxa2 and H2A.Z (Figure S2E). It is interesting that, in contrast to a previous report that loss of H2A.Z-containing nucleosomes occurs mainly at the −1 nucleosome relative to TSSs in human $CD4^+$ T cells (Schones et al., 2008), we found that Foxa2/H2A.Z-enriched nucleosomes were depleted preferentially at promoter, exonic, and 5′UTR regions during ES cell differentiation (Figure S2F). Neither Foxa2 nor H2A.Z were found enriched at partial nucleosome dynamic regions (Figures S2G and S2H). We also analyzed nucleosome depletion and occupation regions surrounding histone H3 methylation sites including H3K4me1, H3K4me2, H3K4me3, H3K9me3, H3K27me3, H3K36me3, and H3K79me3. ChIP-seq data for these markers in undifferentiated mouse ES cells were obtained from the GEO database. We did not find significant correlations between these markers and nucleosome dynamic regions, except for a minor enrichment of nucleosome depletion at H3K4me2 and H3K4me3 sites (data not shown).

Next, we investigated whether Foxa2 and H2A.Z function in nucleosome dynamics is required for the differentiation process. Suppression of either H2A.Z or Foxa2 by RNAi resulted in attenuated nucleosome depletion and impaired ES cell differentiation (Figures 2H and 4A–4E; Figure S3B), suggesting that both H2A.Z and Foxa2 regulate nucleosome depletion during ES cell differentiation and, furthermore, that this process is essential for the differentiation from ES to EHP cells. In addition, overexpression of Foxa2 in undifferentiated ES cells promoted nucleosome depletion (Figures S3C and S3D). Furthermore, to address the causal relationship between nucleosome depletion and Foxa2/H2A.Z binding, we sorted $Foxa2^+$;$ENDM1^-$ cells, in which the Foxa2 gene had been activated but where ES cells had not yet differentiated. In these cells, we indeed found that nucleosome depletion had begun near Foxa2 binding sites (Figure S3E), although nucleosome depletion was partial as compared to fully differentiated cells (Figure 2H). These data suggest that Foxa2/H2A.Z-driven nucleosome depletion occurs prior to ES cell differentiation, a process that is impaired by suppression of either Foxa2 or H2A.Z (Figures 2H and 4). Thus, Foxa2/H2A.Z binding initiates and is required for nucleosome depletion and ES cell differentiation toward endoderm.

Next, we questioned which chromatin remodeling complexes and chaperones might mediate the Foxa2/H2A.Z-dependent nucleosome depletion process. Four ATP-dependent chromatin remodeling complexes, termed SWI/SNF, ISWI, CHD, and INO80/SWR1, have been reported to be involved in embryonic development (Clapier and Cairns, 2009; Kiefer, 2007); and SWR1, together with the chaperone NAP1, mediates the exchange of canonical H2A to the H2A.Z variant in yeast (Mizuguchi et al., 2004). We performed ChIP assays to determine the enrichment of 12 key proteins representing these four complexes in partially differentiated EHP cells (Figure S4). We found that only the nucleosome disassembly/assembly chaperone protein Nap1l1 (the mouse homolog of NAP1), the SWI/SNF complex component Smarca4, and the SWR1 component Kat5 were enriched at nucleosome depletion regions (Figure S4A), which was confirmed by ChIP-seq analysis for Smarc4,

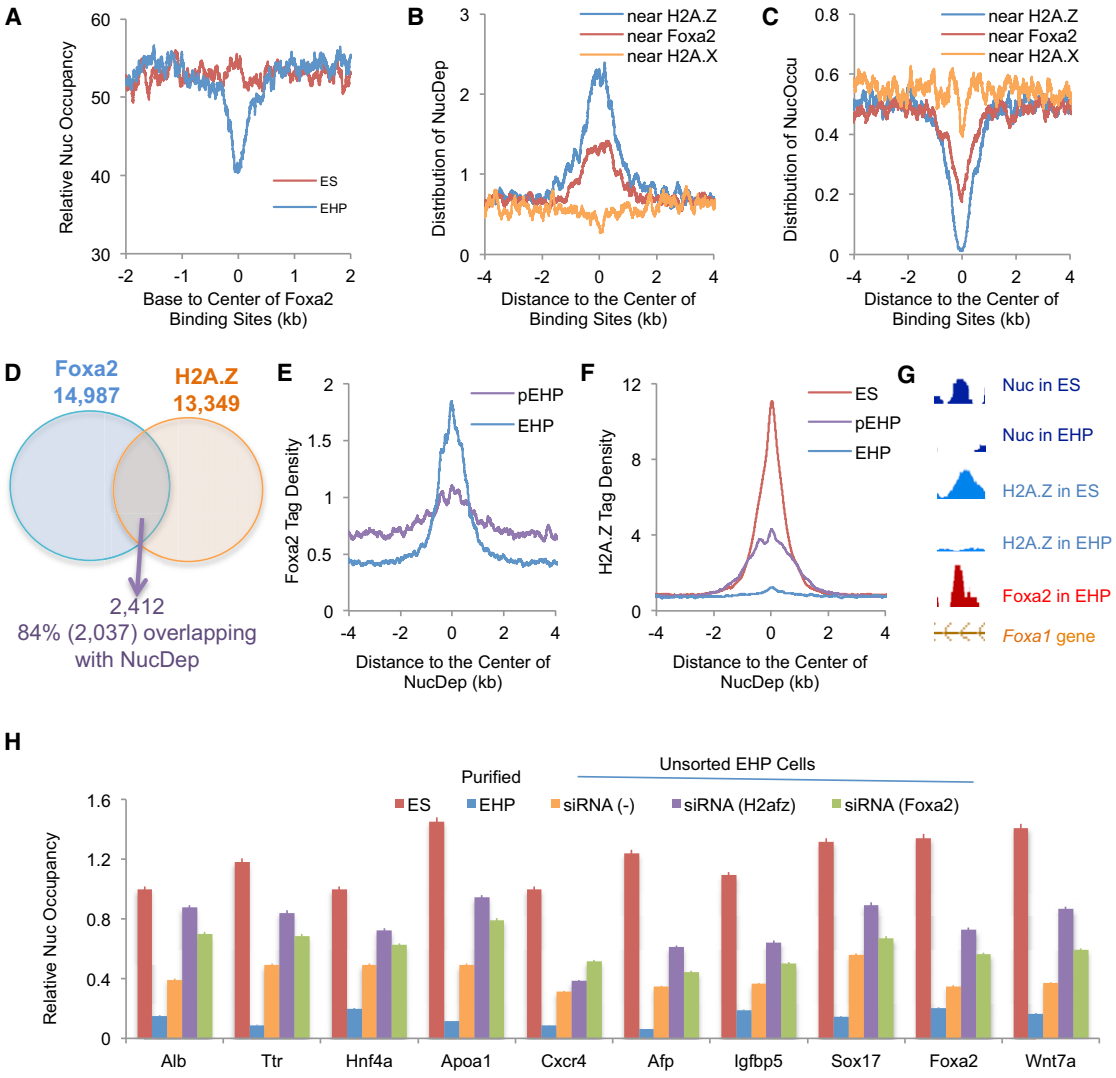

Figure 2. H2A.Z and Foxa2 Are Required for Nucleosome Depletion during ES Cell Differentiation

(A) Nucleosome distribution surrounding Foxa2 binding sites in ES and EHP cells. Note the decrease in nucleosome occupancy at Foxa2 sites in differentiated cells.

(B and C) Genome-wide distribution of nucleosome depletion or occupation regions near H2A.Z, H2A.X, and Foxa2 binding sites.

(D) Cobinding regions of Foxa2 and H2A.Z overlap with nucleosome depletion regions. Foxa2 binding sites were pooled from EHP and pEHP (partially differentiated; see Figure S3A) cells; H2A.Z binding sites were pooled from ES and pEHP cells.

(E and F) Foxa2 and H2A.Z tag density near Foxa2/H2A.Z-associated nucleosome depletion regions.

(G) Colocalization of Foxa2/H2A.Z and nucleosome depletion regions in the intron of the *Foxa1* gene.

(H) Nucleosome depletion during ES cell differentiation is dependent on Foxa2 and H2A.Z. Nucleosome occupancy was determined by qPCR at 10 nucleosome depletion regions that are bound by both H2A.Z and Foxa2 in differentiated ES cells. Relative nucleoscome occupancy is shown for ES cells, sorted EHP cells, unsorted EHP [siRNA (-), scramble siRNA control] cells, and unsorted EHP cells transfected with siRNAs for H2afz (H2A.Z) or Foxa2. Error bars, SEM.

See also Figures S2, S3, S4, and S5.

Kat5, and Nap1l1 (Figures 3A–3C). To investigate whether Foxa2 and H2A.Z form a complex with these chromatin remodelers, as suggested by our genome-wide location analysis, we performed coimmunoprecipitation experiments using differentiated EHP cells. As shown in Figure 3D, all five proteins tested (i.e., Foxa2, H2A.Z, Nap1l1, Kat5, and Smarca4) were found to interact in differentiated EHP cells. In addition, we found that the occupancy of both Smarca4 and Nap1l1 at nucleosome depletion regions was impaired when Foxa2 expression was suppressed by RNAi during ES cell differentiation, whereas the occupancy of Kat5 at nucleosome depletion regions was impaired by H2A.Z suppression (Figure S4C), suggesting that the recruitment of Nap1l1 and Smarca4 relies on Foxa2, whereas that of Kat5 depends on H2A.Z. Suppression of both Foxa2 and H2A.Z simultaneously did not decrease occupancy of Smarca4/Kat5/Nap1l1 at nucleosome depletion regions further but caused

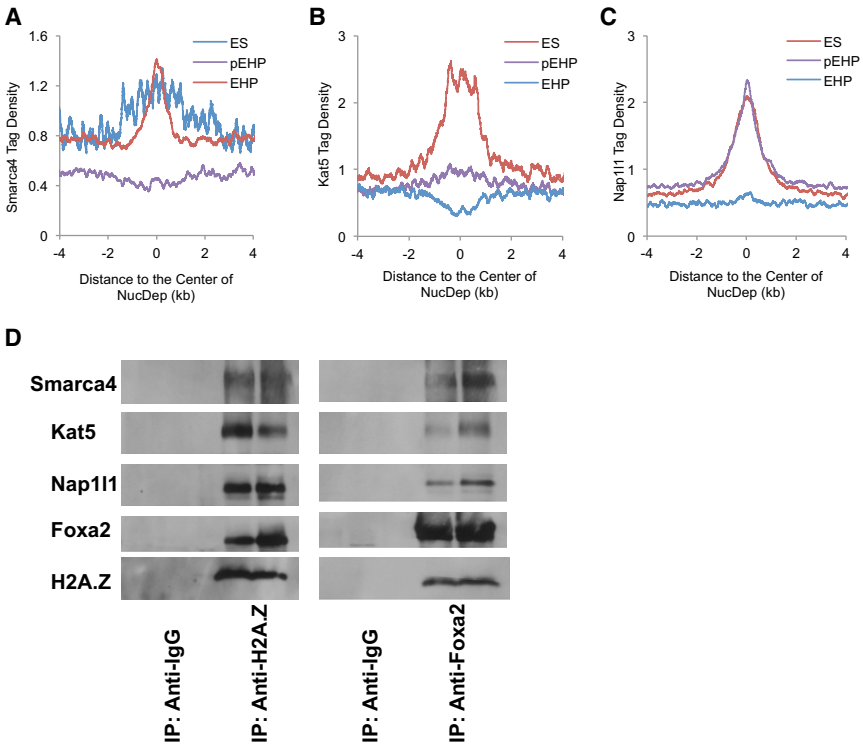

Figure 3. Foxa2/H2A.Z-Driven Nucleosome Depletion complexes during ES cell Differentiation

(A–C) Smarca4 (Brg1), Kat5 (Tip60), and Nap1l1 are enriched at nucleosome depletion regions. The tag density was normalized to 10 million sequencing tags for each sample; bin = 1 bp.

(D) Immunoprecipitation (IP) experiments were performed with differentiated EHP cells using anti-H2A.Z or anti-Foxa2 antibodies, and IP complexes were detected using western blotting with antibodies against Foxa2, H2A.Z, Smarca4, Kat5, and Nap1l1. Anti-igG antibodies were used as negative IP controls.

See also Figures S2, S3, S4, and S5.

a decrease in cell viability (Figures S4C and S5A–S5F). Suppression of Smarca4, Kat5, or Nap1l1, like suppression of Foxa2 and H2A.Z, by RNAi resulted in increased nucleosome occupancy at nucleosome depletion regions and impaired ES cell differentiation (Figures S4D and S5A–S5F). These data suggest that SWI/SNF and INO80 chromatin remodeling complexes cooperate with the chaperone Nap1l1 to enable nucleosome depletion during ES cell differentiation. In summary, our findings support a three-step model for ES cell differentiation into EHP cells: (1) Growth factor-induced cell differentiation initiates Foxa2 expression; (2) Foxa2 binds to nucleosomal DNA on H2A.Z-containing nucleosomes; and (3) Foxa2 and H2A.Z recruit nucleosome disassembly complexes (Nap1l1/SWI/SNF/INO80), enabling nucleosome depletion and cell differentiation (see model in Figure 5E).

DNA Methylation Regulates Nucleosome Occupation during ES Cell Differentiation

DNA methylation at promoters is related to gene silencing, and nucleosomal DNA is relatively more methylated (Chodavarapu et al., 2010). When comparing published DNA methylation profiles of undifferentiated ES cells with our nucleosome maps, we found that nucleosomal DNA fated for disassembly during the differentiation process (i.e., nucleosome depletion regions) was, on average, more methylated than "potential nucleosomal DNA" (i.e., the DNA present in nucleosome occupation regions) (Figures 5A and 5B). However, this correlation was not observed for partial nucleosome dynamic regions (Figure 5B). Using ChIP-quantitative real-time PCR (qPCR) analysis for methylated cytosine, we further showed that nucleosome occupation regions were enriched for methylated DNA in differentiated but not in undifferentiated cells (Figure 5C), indicating that DNA methylation occurred at nucleosome occupation regions during the ES cell differentiation process. To further investigate this notion, we added the DNA methylation inhibitor RG108 to the medium during ES cell differentiation. Inhibition of DNA methylation led not only to reduced nucleosome occupancy but also to impaired ES cell differentiation (Figures 5D and 4F). Together with our gene expression data (Figure 5C; Figure S2A), these findings suggest that DNA methylation is essential for nucleosome occupation and gene silencing during the differentiation from ES to EHP cells. Finially, we examined if chromatin remodelers were also involved in the process of nucleosome occupation during ES cell differentiation. However, none of the twelve chromatin remodeling proteins that we tested was found enriched at nucleosome occupation regions (Figure S4B), suggesting that other mechanisms are involved in this process.

DISCUSSION

Chromatin remodeling plays essential roles in embryonic development. Our findings of epigenetic regulation of H2A.Z occupancy and DNA methylation in nucleosome dynamics during ES cell differentiation provide insights into the dynamics of chromatin structure (Figure 5E). Foxa2, as a "pioneer" factor, is involved in epigenetic regulation of nucleosome remodeling, suggesting the importance of coordinated modulation of epigenetic and genetic regulators in cell fate determination during development. Both nucleosome depletion and occupation occur during ES cell differentiation, indicating that fine-tuning of chromatin structure contributes to lineage-specific gene regulation. Compared to undifferentiated cells, increased nucleosome occupancy in differentiated cells results in a more compact genome and accompanies the switch from pluripotency to differentiated cell functions.

We identified three key chromatin remodeling components, Nap1l1, Smarca4, and Kat5, which were involved in the Foxa2/H2A.Z-mediated process of nucleosome depletion. However, the detailed mechanism of how these components of chromatin

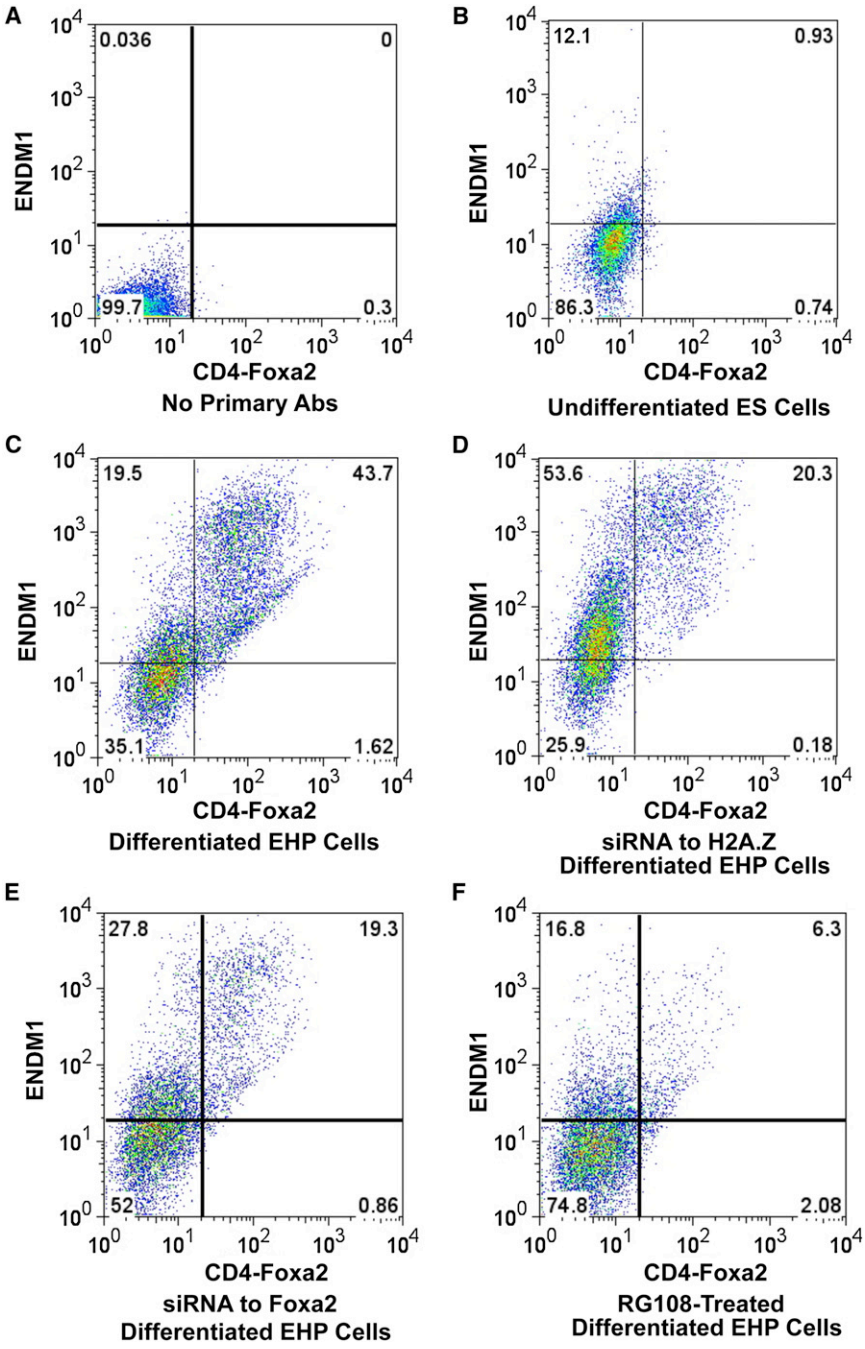

Figure 4. Nucleosome Dynamics and ES Cell Differentiation

Flow cytometry analysis with dual cell surface markers of Foxa2/CD4 and ENDM1 for the assessment of the extent of differentiation.

(A) Control, differentiated ES cells sorted without incubation with primary antibodies.

(B) Undifferentiated ES cells sorted with both antibodies. Less than 1% of the cells are double positive.

(C) Differentiated ES cells, with more than 40% double-positive cells.

(D) ES cells treated with siRNA to H2afz show decreased differentiation potential.

(E) ES cells treated with siRNA to Foxa2 show decreased differentiation potential.

(F) ES cells treated with 100 μM RG108, a DNA methyltransferase inhibitor, exhibit decreased differentiation.

See also Figure S5.

remodeling complexes coordinate to regulate nucleosome disassembly needs to be addressed in future studies. It is interesting that we have not identified any chromatin remodelers that participate in the process of nucleosome occupation, suggesting that nucleosome occupation either is an autonomous process or requires other auxiliary factors. In summary, our detailed genome-wide maps of nucleosome occupancy demonstrate that nucleosomes are dynamic during the differentiation process and that in the case of differentiation toward the endoderm/hepatic fate, nucleosome repositioning is dependent on Foxa2 and H2A.Z. The epigenomic maps reported here constitute an important resource for further integration with additional epigenetic marks and processes that likely contribute to ES cell differentiation.

EXPERIMENTAL PROCEDURES

Mouse ES Cell Differentiation

Undifferentiated mouse ES cells (E14) were differentiated into the EHP fate, as described previously (Gadue et al., 2005; Gadue et al., 2006; Nostro et al., 2008). After 6 days of induction, cells were sorted by flow cytometry with the ENDM1 antibody (an endoderm-specific antibody recognizing a cell-surface protein in endodermal cells) and an engineered cell surface marker, CD4, which is driven by the *Foxa2* promoter. RNA was isolated from these sorted cells. mRNA levels of several marker genes analyzed by qPCR were used to further validate the stage of cell differentiation, including Foxa2, Sox17, HNF4a and HNF6.

Sequencing Nucleosomal and ChIP DNA

Nucleosome and ChIP experiments were carried out as detailed elsewhere (Li et al., 2011). Nuclei were isolated from ES and EHP cells by gradient ultracentrifugation (Greenbaum et al., 1998). Native chromatin without crosslinking was released from nuclei by incubation in a buffer containing 0.1 N $CaCl_2$ and then digested with MNase for 15 min (partial digestion) and 30 min (full digestion) (Morrison et al., 2002). Mononucleosomal DNA was collected and pooled from both partial and full digestion of chromatin. Mononucleosomal and undigested genomic DNA were purified with the QIAGEN PCR purification kit after the digestion with protease K. Sequencing libraries were generated from nucleosomal or ChIP DNA, and sequencing was carried out using the Illumina/Solexa system according to the manufacturer's specifications. For qPCR, undigested genomic DNA was used as input control. Nucleosome occupancy was calculated using $2^{\wedge -(Ct_{nucleosome} - Ct_{input})}$.

ChIP was performed as described previously (Rubins et al., 2005). For ChIP-seq, after crosslinking, chromatin was sonicated to reduce the size of

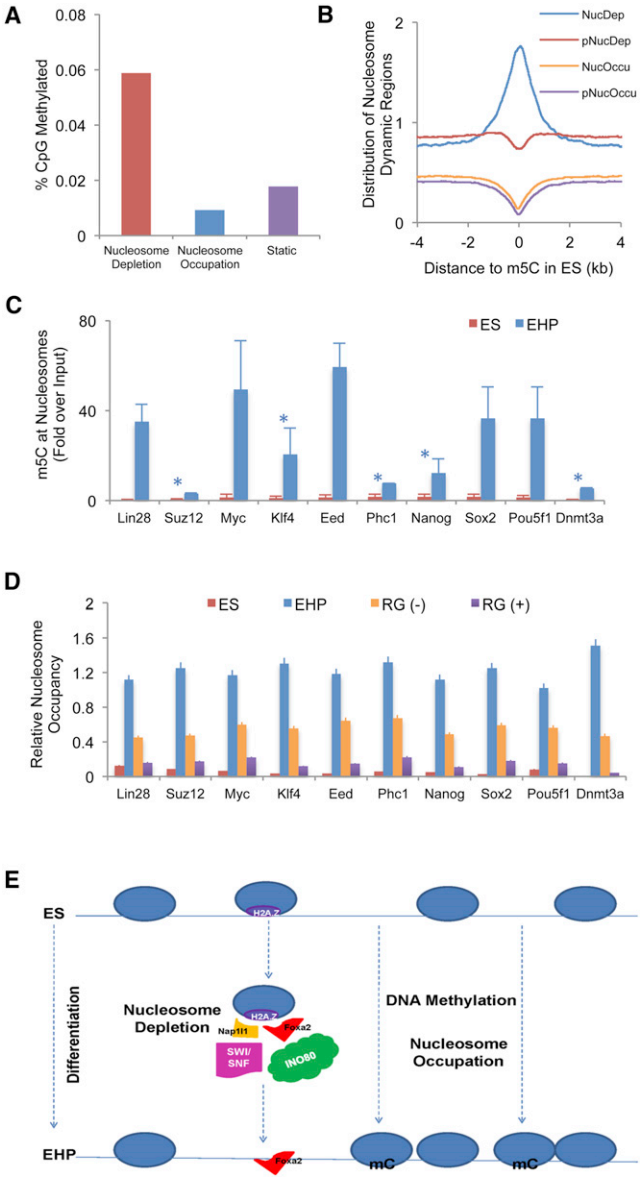

Figure 5. DNA Methylation Promotes Nucleosome Occupation during ES Cell Differentiation

(A) Cytosine DNA methylation profiles in undifferentiated ES cells were obtained from GEO (GSE11304), and compared to our nucleosome maps. The percentage of DNA methylation sites in ES cells is much higher at nucleosome-bound than at nucleosome free regions.

(B) Genome-wide distribution of dynamic nucleosome regions surrounding DNA methylation sites (m5C) in undifferentiated ES cells.

(C) Nucleosomal DNA in ES and EHP cells was immunoprecipitated with an antibody against methylated cytosine (m5C), and DNA methylation was determined by qPCR at genomic regions near key pluripotency maker genes, which are silenced during ES cell differentiation. DNA at these loci is unmethylated in undifferentiated ES cells but shows increased methylation after differentiation. The fold enrichment was normalized to genomic DNA. *$p < 0.05$; all others, $p < 0.01$. Error bars, SEM.

(D) Nucleosome occupancy at nucleosome occupation regions of pluripotency marker genes (the same regions assayed in Figure 5C) in ES cells, sorted EHP cells, unsorted control EHP (RG(−)) cells, and unsorted EHP cells treated with RG108 (RG (+)), a DNA methyltransferase inhibitor. Nucleosome occupancy is severely blunted when DNA methylation is inhibited. Error bars, SEM.

(E) Schematic view of nucleosome dynamics during ES cell differentiation. mC, methylated cytosine. ES represents, specifically, undifferentiated ES cells. See also Figure S4.

DNA to 100 to ~1,000 base pairs (bp), which was further modified for Illumina sequencing. Sequential ChIP for Foxa2 and H2A.Z was performed in both orders. Antibodies used were: Foxa2 (a kind gift of J. Whitsett, Cincinnati, OH, USA), H2A.Z (Abcam, ab4174), H2A.X (Abcam, ab11175), Brg1 (Santa Cruz, sc-8749 and Abcam, ab4081), Tip60 (Santa Cruz, sc-5725 and Abcam, ab23886), and Nap1l1 (Santa Cruz, sc-292698 and Abcam, ab33076). For regular ChIP assays, input and precipitated DNA fragments were subjected to qPCR with primer sets for putative binding sites of Foxa2 and H2A.Z. Enrichment of the targets was calculated using the 28S rRNA locus as a reference and is shown relative to the input chromatin. Three biological replicates for ChIP-qPCR, two biological replicates for ChIP-seq, and pooled three biological replicates for MNase-Seq were analyzed.

Computational Analysis

Nucleosome Occupancy Calculation

Short sequencing reads were mapped to the mouse reference genome (mm8) by ELAND and then subjected to analysis based on Dynamic Analysis of Nucleosome Position and Occupancy by Sequencing (DANPOS; K.C., Yuanxin Xi, Xuewen Pan, Z.L., K.H.K., Jessica Tyler, Sharon Dent, Xiangwei He, and W.L., unpublished data; http://code.google.com/p/DANPOS/). The average size of DNA fragments in each sample was estimated by cross-strand Pearson correlation. The 5′ end of each uniquely mapped and high-quality read was shifted half the fragment size toward the 3′ end, and then extended 50 bp in both directions. Nucleosome occupancy at each base pair was calculated as read coverage. After calculating occupancy for each sample, we performed quantile normalization among all samples.

Nucleosome Calling

Nucleosome positions were first called by using a sliding window of 40 bp to identify a bell-shaped curve supported by at least five reads, with the occupancy summit in the middle of the sliding window. Neighboring bell-shaped curves less than 110 bp distant were merged into one. Each nucleosome was then determined by the summit and neighboring edges of the bell-shaped curve. The edges were determined by searching for the lowest flanking occupancy valleys. We required that the nucleosome edges should be at least 40 bp but no more than 100 bp away from the summit.

Detecting Nucleosome Changes

Sequencing reads were aligned to the mouse reference genome (mm8). Total uniquely aligned reads for each experiment are listed in Table S1. We detected nucleosome occupancy changes based on DANPOS. With the current genome coverage, tag distribution along the genome could be modeled by a Poisson distribution, with one parameter, λ, for both the mean and the variance of the distribution. To estimate the significance of observing nucleosome occupancy at each base pair in a treatment sample, we calculated the p-value-based Poisson distribution, with λ defined by the nucleosome occupancy at the same base pair in a control sample. Then, the Poisson-based p value at each base pair was transformed to a score as $-\log_{10}$ (p value). Differential nucleosome peaks were called from the score data based on the same method used for nucleosome calling.

After nucleosome occupancy was called by DANPOS, the exact nucleosome positions were retrieved from the extended BED files based on the average size of DNA fragments for all nucleosome reads. We identified two dynamic features in the genome where nucleosome positions differed between ES and EHP cells using DANPOS: nucleosome depletion and occupation regions, which were further categorized into four groups: complete nucleosome depletion regions (cNucDep, changing from nucleosome occupied to nucleosome free during the course of differentiation), complete nucleosome occupation regions (cNucOccu, changing from nucleosome free to nucleosome occupied), partial nucleosome depletion regions (pNucDep, changing from high to low tag density at nucleosome positions), and partial nucleosome occupation regions (pNucOccu, changing from low to high tag

density at nucleosome positions). The statistical significance of nucleosome dynamic regions between ES and EHP cells was calculated using a p value of 1e-5 as cutoff. The distribution of nucleosome dynamic regions was analyzed with the BEDTools, HOMER, Cluster 3.0, and Java TreeView algorithms (Quinlan and Hall, 2010). For nucleosome heatmaps near TSS, a data matrix was generated by HOMER (bin = 1 bp), clustered with Cluster 3.0, and visualized by Java TreeView. ChIP-seq data were analyzed with the GLITR and HOMER algorithms using default parameters (Heinz et al., 2010; Tuteja et al., 2009). All relative distributions between two peaks (nucleosome dynamic regions versus binding sites or between two binding sites) and tag density analysis were analyzed by HOMER (bin = 1 bp) (Heinz et al., 2010), from which the relative occupancy was normalized to total reads. The ChIP-seq data sets for histone modifications in undifferentiated mouse ES cells were obtained from the National Center for Biotechnology Information Gene Expression Omnibus (NCBI GEO) database (GSE15884, GSE11724, GSE12241, GSE15814, and GSE11172) (Marks et al., 2009; Marson et al., 2008; Meissner et al., 2008; Mikkelsen et al., 2007).

Gene Expression Microarray

RNA was isolated from ES and EHP cells and reverse transcribed and labeled as described previously (Gao et al., 2009). Fluorescence-labeled cDNAs were hybridized to the Whole Mouse Genome Oligo Microarray (Agilent). This microarray represents over 41,000 mouse gene transcripts. Genes displaying a fold change over 1.5-fold between ES and EHP cells and a false discovery rate less than 10%, calculated using significance analysis of microarray (SAM) analysis, were selected.

Gene Suppression by siRNA

Three sets of siRNA oligos targeted to Foxa2, H2afz, Smarca4, Kat5, and Nap1l1 were purchased from Integrated DNA Technologies. Gene suppression by siRNA was carried out as described (Gadue et al., 2009), with the modification that a mixture of three siRNA oligos for each target was added before inducing cell differentiation. In addition, antibiotics were not added during gene suppression.

Combination Transfection Method for Mouse ES Cells

To improve the transfection efficiency of mouse ES cells, we combined both electroporation and liposome fusion. First, cells were electroporated with a kit specific for mouse ES cells electroporation (Lonza). Then, immediately after electroporation, liposome fusion was applied with the kit of Lipofectamine LTX Plus (Invitrogen). An eGFP expression vector (Lonza) was cotransfected to evaluate the transfection efficiency. Nucleosome occupancy was measured by qPCR as described earlier. Mouse Foxa2 cDNA driven by a CMV promoter was constructed into a pHD vector, which was used to overexpress Foxa2 in mouse ES cells.

Immunoprecipitation of Methylated DNA

To investigate the methylation of nucleosomal DNA, an antimethylated cytosine antibody kit (Epigenetics) was used to pull down methylated nucleosomal DNA after micrococcal nuclease digestion.

Coimmunoprecipitation Experiment

Cell lysates from differentiated EHP cells were incubated with either anti-Foxa2 or anti-H2A.Z antibodies at 4°C overnight. Protein G-coupled Dynabeads (Invitrogen) were used for purification. Proteins were eluted from beads and analyzed by SDS-PAGE and immunoblotting with anti-Foxa2, anti-H2A.Z, anti-Nap1l1, anti-Kat5 and anti-Smarca4 antibodies. Anti-immunoglobulin G (IgG) antibodies were used as negative control in the immunoprecipitation step.

Inhibition of DNA Methylation

The DNA methylation specific inhibitor RG108 (100 μM) (Stemgent) was added to the culture medium during the entire process of ES cell differentiation protocol.

ACCESSION NUMBERS

The Array Express accession number for the expression arrays is E-MTAB-1308, and the accession number for the sequencing data is E-MTAB-1302.

SUPPLEMENTAL INFORMATION

Supplemental Information includes five figures and one table and can be found with this article online at http://dx.doi.org/10.1016/j.cell.2012.11.018.

ACKNOWLEDGMENTS

We thank Dr. Shelley Berger for critical comments on the manuscript, and Alan Fox, Olga Smirnova, Matt Mansh, Aline Disimone, Karrie Brondell, Amber Riblett, and James LaRossa for excellent technical support. We thank Drs. Keji Zhao and Gangqing Hu (National Institutes of Health/National Heart, Lung, and Blood Institute) for helpful suggestions on computational analysis on our nucleosome data. We also thank Dr. Philip Streeter (Oregon) for kindly providing the ENDM1 (G10) antibody. This study was supported by the National Institute of Diabetes and Digestive and Kidney Diseases (P01-DK049210 to K.H.K.). Z.L. was supported by National Science and Engineering Research Council of Canada and Juvenile Diabetes Research Foundation postdoctoral fellowship awards. This study was partially supported by the Cancer Prevention Research Institute of Texas (RP110471-C3 to W.L.). Z.L. and K.H.K. designed the experiments and wrote the manuscript. Z.L. performed the majority of experiments and computational analysis. P.G. and Y.J. did a part of the ES cell culture and sorting. K.C., W.L., G.T., and J.S. contributed to the computational analysis. K.H.K. directed the whole study.

Received: March 9, 2012
Revised: August 30, 2012
Accepted: November 1, 2012
Published: December 20, 2012

REFERENCES

Chodavarapu, R.K., Feng, S., Bernatavichute, Y.V., Chen, P.Y., Stroud, H., Yu, Y., Hetzel, J.A., Kuo, F., Kim, J., Cokus, S.J., et al. (2010). Relationship between nucleosome positioning and DNA methylation. Nature *466*, 388–392.

Clapier, C.R., and Cairns, B.R. (2009). The biology of chromatin remodeling complexes. Annu. Rev. Biochem. *78*, 273–304.

Gadue, P., Huber, T.L., Nostro, M.C., Kattman, S., and Keller, G.M. (2005). Germ layer induction from embryonic stem cells. Exp. Hematol. *33*, 955–964.

Gadue, P., Huber, T.L., Paddison, P.J., and Keller, G.M. (2006). Wnt and TGF-beta signaling are required for the induction of an in vitro model of primitive streak formation using embryonic stem cells. Proc. Natl. Acad. Sci. USA *103*, 16806–16811.

Gadue, P., Gouon-Evans, V., Cheng, X., Wandzioch, E., Zaret, K.S., Grompe, M., Streeter, P.R., and Keller, G.M. (2009). Generation of monoclonal antibodies specific for cell surface molecules expressed on early mouse endoderm. Stem Cells *27*, 2103–2113.

Gao, N., White, P., and Kaestner, K.H. (2009). Establishment of intestinal identity and epithelial-mesenchymal signaling by Cdx2. Dev. Cell *16*, 588–599.

Gouon-Evans, V., Boussemart, L., Gadue, P., Nierhoff, D., Koehler, C.I., Kubo, A., Shafritz, D.A., and Keller, G. (2006). BMP-4 is required for hepatic specification of mouse embryonic stem cell-derived definitive endoderm. Nat. Biotechnol. *24*, 1402–1411.

Greenbaum, L.E., Li, W., Cressman, D.E., Peng, Y., Ciliberto, G., Poli, V., and Taub, R. (1998). CCAAT enhancer- binding protein beta is required for normal hepatocyte proliferation in mice after partial hepatectomy. J. Clin. Invest. *102*, 996–1007.

Heinz, S., Benner, C., Spann, N., Bertolino, E., Lin, Y.C., Laslo, P., Cheng, J.X., Murre, C., Singh, H., and Glass, C.K. (2010). Simple combinations of lineage-determining transcription factors prime cis-regulatory elements required for macrophage and B cell identities. Mol. Cell *38*, 576–589.

Ho, L., and Crabtree, G.R. (2010). Chromatin remodelling during development. Nature *463*, 474–484.

Jiang, C., and Pugh, B.F. (2009). Nucleosome positioning and gene regulation: advances through genomics. Nat. Rev. Genet. *10*, 161–172.

Kiefer, J.C. (2007). Epigenetics in development. Dev. Dyn. *236*, 1144–1156.

Lee, C.S., Friedman, J.R., Fulmer, J.T., and Kaestner, K.H. (2005). The initiation of liver development is dependent on Foxa transcription factors. Nature *435*, 944–947.

Lee, T.I., Jenner, R.G., Boyer, L.A., Guenther, M.G., Levine, S.S., Kumar, R.M., Chevalier, B., Johnstone, S.E., Cole, M.F., Isono, K., et al. (2006). Control of developmental regulators by Polycomb in human embryonic stem cells. Cell *125*, 301–313.

Li, Z., Schug, J., Tuteja, G., White, P., and Kaestner, K.H. (2011). The nucleosome map of the mammalian liver. Nat. Struct. Mol. Biol. *18*, 742–746.

Marks, H., Chow, J.C., Denissov, S., Françoijs, K.J., Brockdorff, N., Heard, E., and Stunnenberg, H.G. (2009). High-resolution analysis of epigenetic changes associated with X inactivation. Genome Res. *19*, 1361–1373.

Marson, A., Levine, S.S., Cole, M.F., Frampton, G.M., Brambrink, T., Johnstone, S., Guenther, M.G., Johnston, W.K., Wernig, M., Newman, J., et al. (2008). Connecting microRNA genes to the core transcriptional regulatory circuitry of embryonic stem cells. Cell *134*, 521–533.

Mavrich, T.N., Jiang, C., Ioshikhes, I.P., Li, X., Venters, B.J., Zanton, S.J., Tomsho, L.P., Qi, J., Glaser, R.L., Schuster, S.C., et al. (2008). Nucleosome organization in the Drosophila genome. Nature *453*, 358–362.

McPherson, C.E., Shim, E.Y., Friedman, D.S., and Zaret, K.S. (1993). An active tissue-specific enhancer and bound transcription factors existing in a precisely positioned nucleosomal array. Cell *75*, 387–398.

Meissner, A., Mikkelsen, T.S., Gu, H., Wernig, M., Hanna, J., Sivachenko, A., Zhang, X., Bernstein, B.E., Nusbaum, C., Jaffe, D.B., et al. (2008). Genome-scale DNA methylation maps of pluripotent and differentiated cells. Nature *454*, 766–770.

Mikkelsen, T.S., Ku, M., Jaffe, D.B., Issac, B., Lieberman, E., Giannoukos, G., Alvarez, P., Brockman, W., Kim, T.K., Koche, R.P., et al. (2007). Genome-wide maps of chromatin state in pluripotent and lineage-committed cells. Nature *448*, 553–560.

Mizuguchi, G., Shen, X., Landry, J., Wu, W.H., Sen, S., and Wu, C. (2004). ATP-driven exchange of histone H2AZ variant catalyzed by SWR1 chromatin remodeling complex. Science *303*, 343–348.

Morrison, A.J., Sardet, C., and Herrera, R.E. (2002). Retinoblastoma protein transcriptional repression through histone deacetylation of a single nucleosome. Mol. Cell. Biol. *22*, 856–865.

Nostro, M.C., Cheng, X., Keller, G.M., and Gadue, P. (2008). Wnt, activin, and BMP signaling regulate distinct stages in the developmental pathway from embryonic stem cells to blood. Cell Stem Cell *2*, 60–71.

Quinlan, A.R., and Hall, I.M. (2010). BEDTools: a flexible suite of utilities for comparing genomic features. Bioinformatics *26*, 841–842.

Raisner, R.M., Hartley, P.D., Meneghini, M.D., Bao, M.Z., Liu, C.L., Schreiber, S.L., Rando, O.J., and Madhani, H.D. (2005). Histone variant H2A.Z marks the 5′ ends of both active and inactive genes in euchromatin. Cell *123*, 233–248.

Rubins, N.E., Friedman, J.R., Le, P.P., Zhang, L., Brestelli, J., and Kaestner, K.H. (2005). Transcriptional networks in the liver: hepatocyte nuclear factor 6 function is largely independent of Foxa2. Mol. Cell. Biol. *25*, 7069–7077.

Schones, D.E., Cui, K., Cuddapah, S., Roh, T.Y., Barski, A., Wang, Z., Wei, G., and Zhao, K. (2008). Dynamic regulation of nucleosome positioning in the human genome. Cell *132*, 887–898.

Shivaswamy, S., Bhinge, A., Zhao, Y., Jones, S., Hirst, M., and Iyer, V.R. (2008). Dynamic remodeling of individual nucleosomes across a eukaryotic genome in response to transcriptional perturbation. PLoS Biol. *6*, e65.

Tuteja, G., White, P., Schug, J., and Kaestner, K.H. (2009). Extracting transcription factor targets from ChIP-Seq data. Nucleic Acids Res. *37*, e113.

Valouev, A., Ichikawa, J., Tonthat, T., Stuart, J., Ranade, S., Peckham, H., Zeng, K., Malek, J.A., Costa, G., McKernan, K., et al. (2008). A high-resolution, nucleosome position map of C. elegans reveals a lack of universal sequence-dictated positioning. Genome Res. *18*, 1051–1063.

Zaret, K. (1999). Developmental competence of the gut endoderm: genetic potentiation by GATA and HNF3/fork head proteins. Dev. Biol. *209*, 1–10.